AIP Advances

Large-area patterning of sub-100 nm epitaxial L10 FePt dots array via nanoimprint lithography

Zheng Li, Wei Zhang, and Kannan M. Krishnan

Citation: AIP Advances **5**, 087165 (2015); doi: 10.1063/1.4929578
View online: http://dx.doi.org/10.1063/1.4929578
View Table of Contents: http://scitation.aip.org/content/aip/journal/adva/5/8?ver=pdfcov
Published by the AIP Publishing

Large-area patterning of sub-100 nm epitaxial $L1_0$ FePt dots array via nanoimprint lithography

Zheng Li, Wei Zhang,[a] and Kannan M. Krishnan[b]
Department of Materials Science and Engineering, University of Washington, Seattle, WA 98195, USA

(Received 3 July 2015; accepted 13 August 2015; published online 21 August 2015)

Bit-patterned media, a promising candidate for next generation high density magnetic recording, requires sub-100 nm dots array on a wafer scale, a high degree of patterning control of the size distribution, and a material with high perpendicular anisotropy. In this work, large area (0.75 cm × 0.75 cm) dots array was achieved by nanoimprint lithography and ion milling from $L1_0$ FePt thin films that are pre-sputtered at 450 °C with both high crystalline quality and good chemical order. The sub-100 nm dots are decoupled from each other and show both narrow size distributions and high coercivity values on the order of 11 kOe. Our work would cast light for the application of bit-patterned media. [http://dx.doi.org/10.1063/1.4929578]

INTRODUCTION

Ultrahigh-density magnetic recording is a continuously evolving technology. For perpendicular magnetic recording (PMR), the projected upper limit of ~1 Tb/in^2 is expected to be reached soon due to the superparamagnetic effect,[1] where the median grain size on the recording media becomes unstable due to thermal fluctuation. To address this issue, several approaches have been proposed, including heat-assisted magnetic recording (HAMR),[2] exchange-coupled composite (ECC)[3] media and bit-patterned media (BPM).[4] Among these, BPM appears to be promising for ultrahigh-density towards 10 Tb/in^2. For traditional PMR, a "bit" of information is stored by a collection of grains, where the signal to noise ratio (SNR) is given by SNR = 10 × log(N) dB, with N being the average number of grains per bit.[5] For BPM, however, each bit is represented by only one patterned element. Thus, the volume of each individual bit/dot determines the energy barrier against thermal fluctuation and enables much higher storage density. However, there are several obstacles, such as synchronized writing/reading process[6] and air-bearing control between head/media,[7] that need to be overcome before this technology matures.

From the media point of view, there are two critical issues facing BPM. First, it requires a magnetic material with high perpendicular anisotropy;[8,9] $L1_0$ FePt with the *c*-axis as the magnetic easy axis and normal to the film plane is promising.[10] However, $L1_0$ FePt is typically deposited under elevated temperatures (~ 800°C, for instance[11]) in order to achieve good chemical ordering; but this is impractical because of large surface roughness due to grain growth at high temperature and a nanoparticulate morphology[11] which generates unfavorable boundary domain-wall pinning sites. There have been several reports on lower temperature fabrication of $L1_0$ FePt thin films.[12–15] All of them relies on either compositional change of FePt binary alloy[12,13] or different types of seed layers.[14,15] Thus, lower $L1_0$ FePt growth temperature without compositional change or seed layer is desired. Second, the top-down design and fabrication of BPM requires high quality and cost effective lithographical patterning;[16] both narrow dot size and to a lesser extent shape variations, and large patterning area are critical for real application. With each bit represented by only one patterned

[a]present address: Argonne National Laboratory, Lemont, IL 60439
[b]Corresponding Author: kannanmk@uw.edu

dot, any fabrication defects would lead to amplified noise in BPM compared to the traditional PMR media, and would be directly reflected in a higher bit-error rate (BER).[17] As a result, a high quality patterning technique is required. It has been reported that any dot *shape* fluctuation only contribute a second-order disturbance and can be neglected.[17] However, the dot *size* fluctuation is predicted to be critical[18] and narrow distribution (dot-size standard deviation, $\sigma < 10\%$) is required for densities larger than $1Tb/in^2$.[6] One promising approach is nanoimprint lithography (NIL),[19] with advantages of high resolution, high throughput, low cost, and wafer scale fabrication.[20] However, the NIL patterning quality is not yet optimized at the sub-100nm length scale and few studies[11,21–23] have been reported on epitaxial $L1_0$ FePt dots array with good dot-size distribution.

Here, we describe the fabrication of $L1_0$ ordered FePt films at a lower growth temperature (450 °C), with high crystalline quality and perpendicular magnetic anisotropy. Then, large-area (0.75 cm × 0.75 cm) dots array is fabricated using NIL combined with Molybdenum mask-transfer and ion milling. The sub-100 nm dots array shows high coercivity and is characterized by magnetic force microscopy (MFM) and vibrating sample magnetometer (VSM). The magnetization reversal mechanism is studied by d.c. demagnetizing curves.

EXPERIMENTAL METHODS

FePt films were prepared by ultra-high-vacuum ion beam sputtering (UHV-IBS)[24,25] using a $Fe_{50}Pt_{50}$ (at.%) alloy target with a base pressure lower than 5×10^{-8} torr. An epitaxial $L1_0$ FePt film with 15nm-thickness was deposited at a rate of 1.5Å/s onto MgO (001) single crystal substrate at 450°C. *In situ* annealing (1h) at the growth temperature was performed right after the deposition. The samples were then cooled down to room temperature and capped with a 3nm-thick Au layer in the vacuum chamber to prevent any surface oxidation.

Subsequent to the thin film deposition, large area patterning was carried out by nanoimprint lithography (NIL) using a Molybdenum mask-transfer lithography process. The transparent quartz master mold for NIL was bought from NTT-AT.[26] It has nanodots array, with elements 100 nm in diameter, and a periodicity of 200 nm, on a total scale of 0.75 cm × 0.75 cm. To extend the life of the master mold, daughter molds for subsequent NIL use were fabricated through duplication from the master mold using Ormostamp (Microresist Tech., GmBH)— a standard procedure developed by our group, which is discussed in detail elsewhere.[27] The schematic of the NIL process is shown in figure 1(a)-1(g).[28–30] First, the desired heterostructures were deposited by UHV-IBS. Then, polymeric resist LOR1A (MicroChem Corp., Newton, MA) was spin-coated onto the sample surface for building the undercut profile, followed by thermal imprint resist 7010R (Microresist Tech., GmBH) coating. The thickness of the bilayer resist, *i.e.* LOR1A (90 nm) / 7010R (120 nm),[31] was optimized for our feature size of sub-100 nm dots array. Next, the coated wafer was thermally imprinted in a Nanonex NX-B100 compact thermal imprinter at 200 psi / 120 °C for a duration of 60 s. Then, RIE dry etching was performed for 25 s followed by wet development (10 s) using TMAH for selectively etching the LOR1A and achieving the undercut, as shown in figure 1(h). Then, 20 nm-thick Molybdenum was deposited at room temperature for mask transfer before lift-off using Remover-PG [figure 1(i)]. Then, the sample was ion-milled in Ar plasma for 25 s to achieve isolated FePt dots. Finally, all Mo-residue on top of the dots was removed by 30% H_2O_2. Figure 1(j) shows the morphology of the FePt dots array.

The crystallographic structures of both film and dot samples were investigated by X-ray diffraction (XRD) θ-2θ scan using Cu K_α radiation. Magnetic measurements were performed on a Quantum Design® physical property measurement system (PPMS) using the VSM mode. The morphology of the samples was studied using scanning electron microscopy (SEM) and atomic force microscopy (AFM). The magnetic microstructure was investigated by MFM using 100 nm CoCr coated high moment probes with a lift height of 40 nm.

RESULTS AND DISCUSSION

A large patterned area, > 0.75 cm × 0.75 cm (same dimensions as the stamp), was achieved. The microscope image [inset in figure 2(a)] demonstrates the large area patterning. Next, we

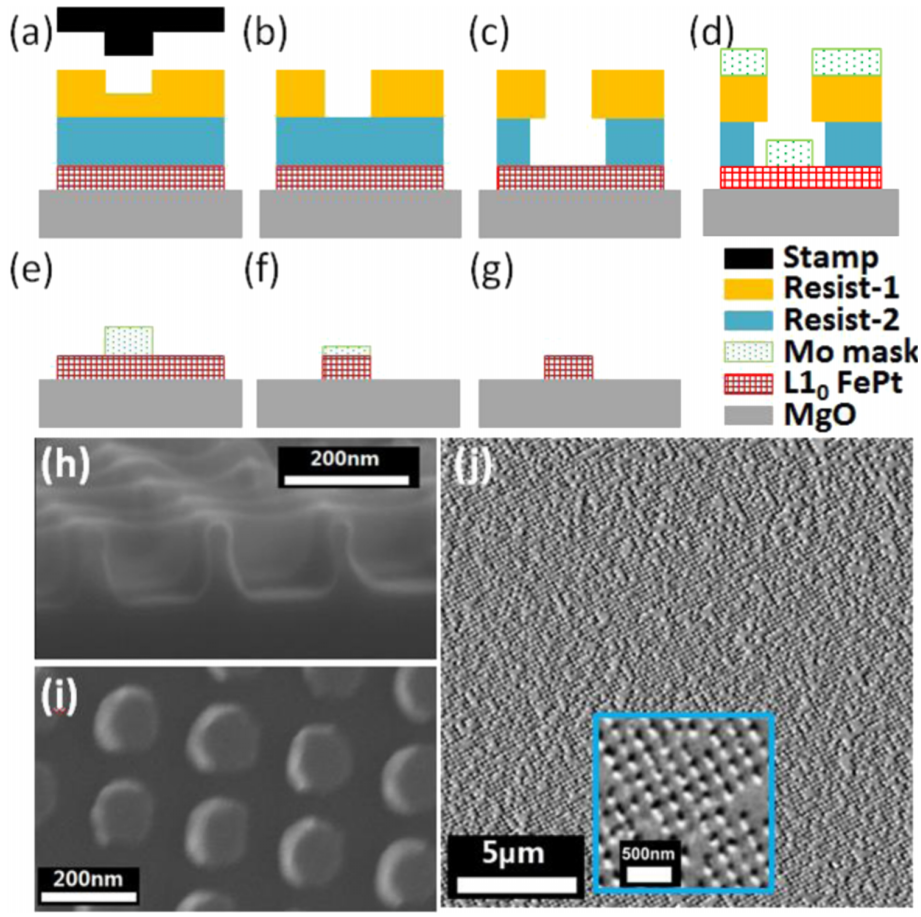

FIG. 1. (a)-(g) Schematic of the nanofabrication process using nanoimprint lithography: (a) thermal imprinting, (b) RIE dry etching, (c) TMAH wet etching, (d) Mo deposition, (e) lift-off, (f) ion milling, and (g) Mo-residual removal by H_2O_2. (h) Cross-sectional SEM image of the bilayer resist undercut profile. (i) Top-down SEM of the Mo dots after resist lift-off. (j) AFM image of FePt dots array morphology.

measured the dot-size distribution using a randomly-picked area of 10 μm × 10 μm, consisting of ~2500 dots, as shown in figure 2(a). The mean size of the dot diameter was analyzed to be 97.7 nm with a standard deviation, σ = 8.3%, that is below the 10% threshold required for high density recording application[6] [figure 2(b)]. The same analysis was also performed in another

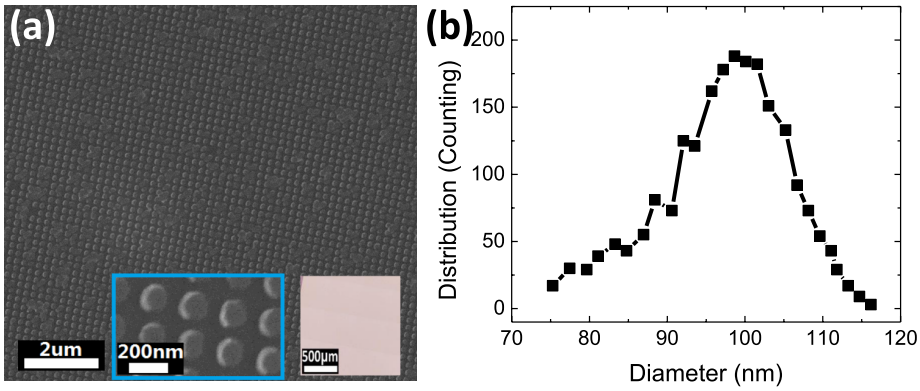

FIG. 2. (a) SEM image of dots array before ion milling. (b) Dot size distribution with average diameter of 97.7 nm. Inset of figure 2(a) shows both outline of the sub-100 nm dots and microscope image of the large area patterning.

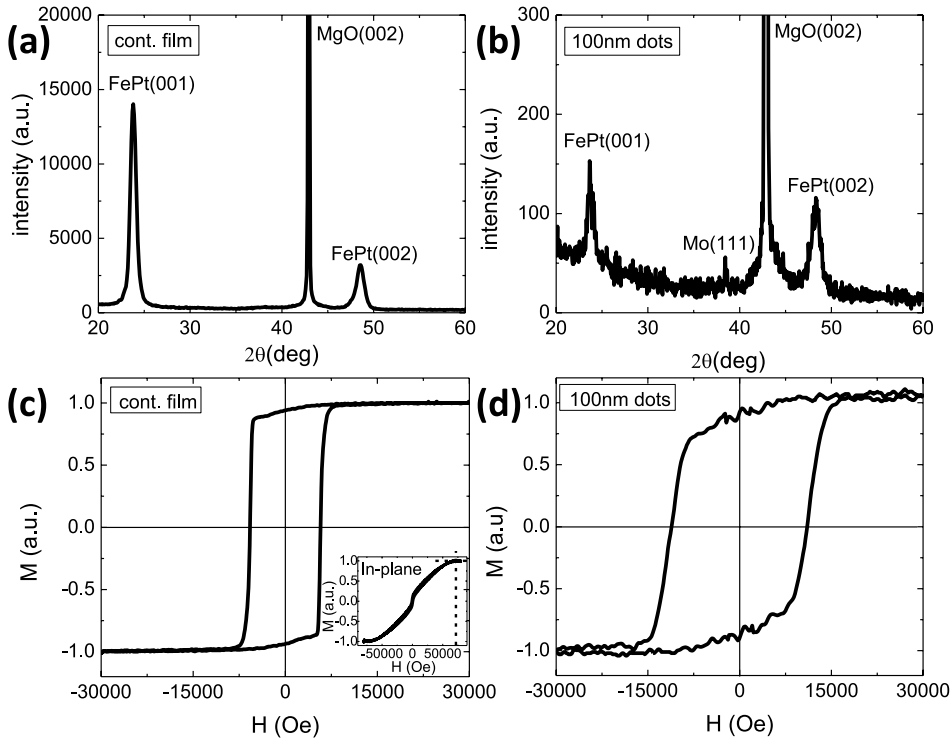

FIG. 3. (a)&(b) XRD θ-2θ scan for both film/dots samples, showing clear $L1_0$ (001) and (002) peaks. Mo (111) peak was observed only in the dot sample (b), suggesting small amount of residual Mo after removal. (c)&(d) Hysteresis loops for both samples. An increased coercivity was observed for patterned dots array sample.

randomly-picked area, with similar results suggesting a consistency in the dot-size distribution. Thus, our NIL fabrication process of sub-100nm dots array is suitable for high-density BPM owing to both large patterning area and good dot-size distribution.

Figure 3(a)&3(b) shows the XRD θ-2θ scans for both film and dot samples. Clear FePt $L1_0$ (001) and (002) peaks were observed, in addition to the MgO (002) peak, indicating good chemical ordering. The peak intensity ratio (I_{001}/I_{002}), widely used as an indicator for the degree of $L1_0$ chemical ordering,[32] decreased after patterning (from 4.74 in thin film to 1.03 in nanodots), which is attributed to the processing in the nanofabrication and will be discussed later.

Next, hysteresis loop measurements were carried out, as shown in figure 3(c)&3(d). For the film sample, a highly-square loop is observed giving a coercivity value of $H_c^{film} = 5.8$ kOe. The sharp reversal process indicates a collective switching triggered by domain wall (DW) nucleation and propagation. To further confirm this argument, we studied the domain pattern during the switching process by MFM. After a.c. demagnetization, a maze-like domain pattern was observed [figure 4(a)], with balanced positive and negative magnetizations, which is typical for perpendicular magnetic anisotropy (PMA) system with strong in-plane exchange coupling.[33] However, when an external field of 6 kOe was applied and then removed after saturation in the opposite direction, an asymmetric domain pattern with significant expansion of the domains in the applied field direction was observed [figure 4(b)]. Moreover, a close loop was observed with a saturation field of $H_{sat.inpl.} = 75$ kOe when the field was applied parallel to the sample surface [inset of figure 3(c)]. This field, along the hard axis, is often referred to as anisotropy field,[34] H_a, and can be used to calculate the magnetic anisotropy constant, K_u. Based on $H_a = 75$ kOe and $M_s = 1140$ emu/cc, we get $K_u = 4.3 \times 10^7\, erg/cc$ and $D_{sd} = 1.4\frac{4\sqrt{AK_u}}{{M_s}^2} = 275\, nm$ for our thin film sample, where D_{sd} is the single domain limit and $A = 10^{-6}$ erg/cm is the exchange stiffness. These results are in good agreement with the theoretical value of ${K_u}^{the.} = 6.6 \times 10^7$ erg/cc and ${D_{sd}}^{the.} = 340$ nm for bulk $L1_0$ FePt;[35] thus, our film sample showing high crystalline quality in thin film form is a good candidate for perpendicular magnetic recording (PMR). In short, we fabricated a high anisotropy $L1_0$ FePt

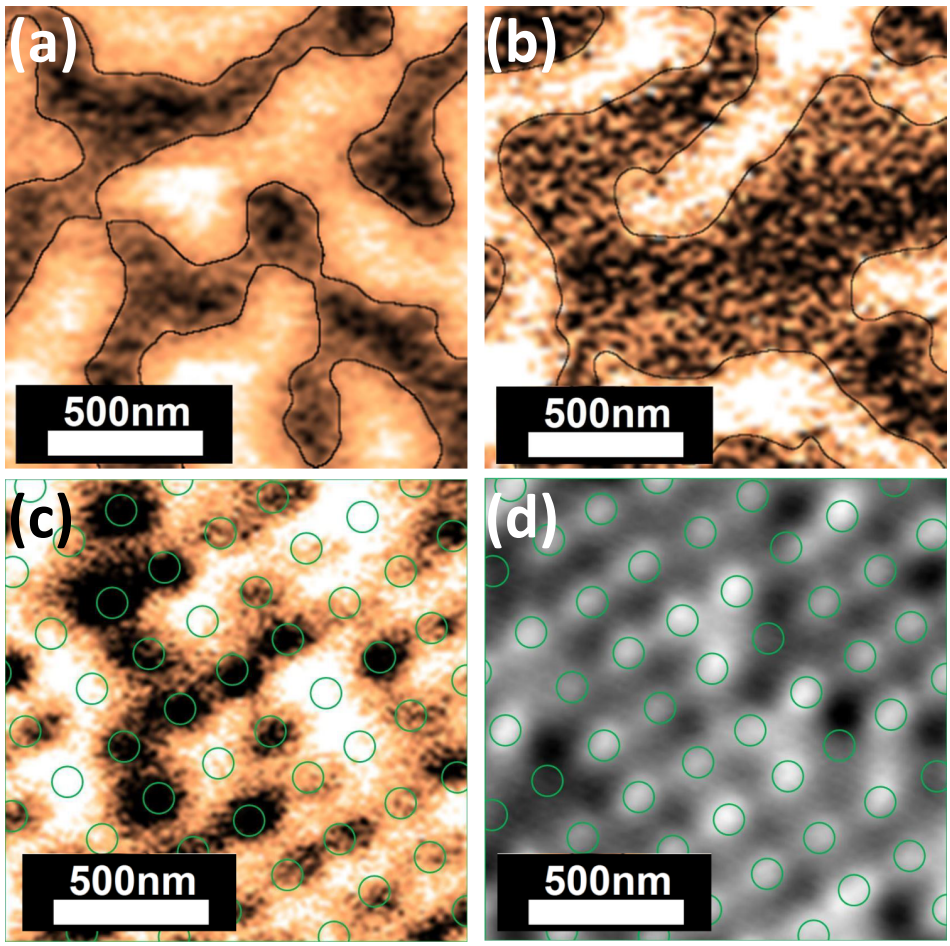

FIG. 4. MFM image of the film sample at remnant states: (a) after a.c. demagnetization, and (b) when an external field of 6 kOe was applied after saturation from the opposite direction. A clear domain wall expansion along the field direction is observed. For the dots array sample: (c) MFM image of dots array after a.c. demagnetization and (d) the corresponding AFM image showing the morphology of the patterned dots.

film where the magnetic reversal is predominantly by domain wall motion, and indicates a strong in-plane exchange coupling.

After NIL patterning, the sub-100 nm dots array showed almost double the coercivity, *i.e.* H_c^{dots} = 11.1 kOe in the out-of-plane direction. This increased coercivity is attributed to patterning effect where the dots are within the single domain limit and therefore DW propagation, being energetically unfavorable, would be prohibited.[36] This argument was confirmed by the MFM imaging. Figure 4(c)&4(d) show the MFM image after a.c. demagnetization and corresponding AFM image of the dots array. The separate white/black regions indicate up/down magnetic domains, suggesting isolated nanodots after ion-milling. We surmise that this isolation breaks down the exchange coupling between dots and increases the coercivity. Next, it is worth discussing the potential integration of this sub-100 nm dots array into current recording mechanism. The head writing field has a theoretical upper limit of 24 kOe due to the intrinsic nature of pole material.[18] In practice, owing to the head design and leakage of magnetic flux, this field could be even smaller,[37] and it is reasonable to assume the short-time head field to be 14 kOe.[38] Nevertheless, the sub-100 nm dots array demonstrated here could fit well into the current writing capability in magnetic recording.

Ion milling has been reported to damage the crystalline structure at the dot surface due to Ar^+ ion bombardment,[23,39,40] and cause a soft magnetic rim. This edge damage is expected in our dot sample, as suggested by the decreased peak intensity ratio (I_{001}/I_{002}) in the XRD data [figure 3(a)&3(b)]. However, this damage will only contribute a very limited fraction of the soft

phase to the high anisotropic volume and won't affect its performance,[41] given that the anisotropy field for the dot sample was measured to be as high as $H_a = H_{sat.inpl.} = 65$ kOe, indicating $K_u = 3.7 \times 10^7 erg/cc$. In short, without sacrificing much of the magnetic stability by the edge damage introduced by ion milling, the high energy barrier for magnetic reversal is retained.

Additionally, it is of interest to discuss the film thickness and its influence on the magnetic properties. First, demagnetizing energy favors thicker sample with perpendicular anisotropy since magnetic "poles" on the top and bottom surface are further apart from each other. However, it cannot be too thick either. In addition to the cost considerations, a too-thick magnetic media would trigger incoherent reversal by thermally injecting a perpendicular DW into the column. Richter argued[18] that the critical thickness, L_T, is determined by $E_{dw} = E_{coh}$ (*), where domain wall energy $E_{dw} = \pi D^2 \sqrt{AK_u}$ is comparable to the energy barrier for coherent rotation $E_{coh} = K_u(\frac{\pi}{4}D^2)L_T$, where D is the dot diameter. However, besides the domain wall energy, the incoherent rotation would also generate another pair of magnetic poles and correspondingly increase the magnetostatic energy, E_{ms}. For our patterned dots with very low aspect ratio ($L_T/D = 15\%$), it is reasonable to assume that the out-of-plane demagnetizing factor $N_Z = 4\pi$. Thus we can rewrite the formula (*) as $E_{dw} + \Delta E_{ms} = E_{coh}$, where $\Delta E_{ms} = 2\pi M_s^2(\frac{\pi}{4}D^2)L_T$ and calculate the critical thickness to be $L_T = 8.5$ nm, which means a domain wall can be thermally injected when the patterned dots are thicker than 8.5 nm. It corresponds to an energy barrier required for a domain wall into a cylinder grain: $E_{barrier} = (E_{dw} + \Delta E_{ms})|_{L_T=8.5\,nm} = E_{coh}|_{L_T=8.5\,nm} = 2.47 \times 10^{-9} erg$. This domain wall injection is unlikely to happen for our 15 nm-thick dots array. To trigger the incoherent rotation from a thermal activation, an energy of $2.47 \times 10^{-9} erg$ that equals $6 \times 10^4 (k_B T_0)$ is required, where k_B is the Boltzmann constant and T_0 is room temperature; this is unlikely to happen.

To further reveal the influence of patterning on the reversal process of film samples, we measured d.c. demag curves which, by measuring the remanence states, illustrates the direct-field demagnetization after saturation opposite to the applied field direction.[42] As a result, the departure of the d.c. demag curve from the descending branch of the major hysteresis loop gives the reversible part of magnetic switching. As shown in figure 5(a)&5(c), both thin film and NIL patterned

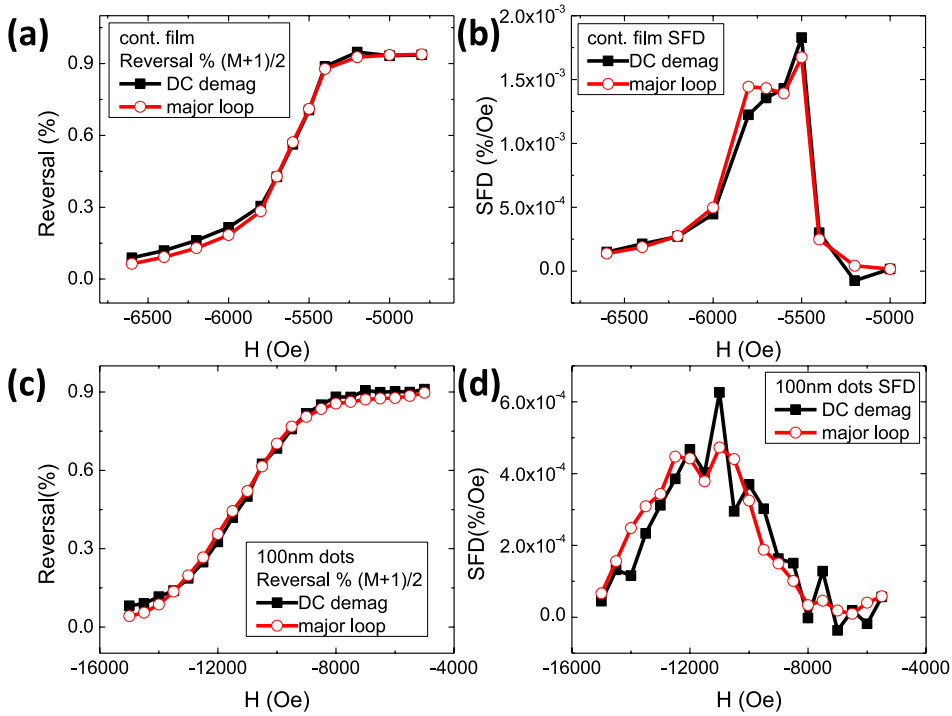

FIG. 5. (a) Comparison of the descending branch of the major loop and the d.c. demag curve of the film sample and (b) first derivative, dM/dH of the both the d.c. demag curves and the descending branch of the hysteresis loops, to illustrate the switching field distribution. (c)&(d) the same set of measurements for the dots array sample.

samples show almost overlapping d.c. demag curves/major loops, indicating that irreversible switching dominates.

Next, the first derivative, $^{dM}/_{dH}$ of both the d.c. demag curves and the descending branch of major loops, was carried out to study the switching field distribution (SFD). There are two points worth mentioning here. First, a slightly narrower SFD was observed in d.c. demag curve for both film and dot samples: the full-width-half-maximum (FWHM) drops from 460 Oe to 415 Oe for the film sample (9.8%) and from 4210 Oe to 3956 Oe for dot sample (6.0%). This narrowing, less than 10%, suggests a more collective behavior of irreversible switching when its complementary part, the reversible switching, was eliminated. This small fraction of reversible switching can be attributed to the magnetostatic interactions between dots which causes a shallower loop with broadened SFD[18] and can be partially released with the assistance of a soft under layer (SUL).[41] Second, compared to the thin film [figure 5(b)], the dots array [figure 5(d)] exhibits a very large increase in SFD; almost ten-time larger FWHM was observed in the patterned dots. This increase in SFD is a result of individual switching mechanism of the decoupled dots and processing-related defects, such as dots alignment issue from patterning and edge damage from ion milling.[23,39,40] Additionally, the expanded SFD could also possibly arise from the variation of K_u in the film,[36] which could be extrinsically expressed if there is only one possible nucleation center per patterned dot.[43] In summary, even though these results are promising for BPM, the SFD for the patterned dots array should be further narrowed down to optimize their performance. Future study, such as the introduction of a top soft magnetic layer to establish exchange-spring behavior[44] and facilitate uniform switching[45] within dots array, will be carried out.

CONCLUSION

In conclusion, we have fabricated sub-100 nm FePt dots array over a large patterning area. The 15 nm-thick films showed good $L1_0$ chemical ordering. The reversal process was dominated by domain wall expansion. Sub-100 nm dots array from the $L1_0$ FePt film with good size uniformity was fabricated using nanoimprint lithography. A higher coercivity of 11.1 kOe with a broadened switching field distribution were observed in dots array. Further work will be focused on enhancing the magnetization reversal uniformity after patterning with higher dot density and transferring the procedure onto glass substrates for BPM application.

ACKNOWLEDGEMENT

This work was supported by NSF-DMR under Grant No. 1063489. Part of this work was conducted at the University of Washington-Washington Nanofabrication Facility (UW WNF), a national user facility that is part of the National Nanotechnology Infrastructure Network (NNIN). Z.L. would like to acknowledge China Scholarship Council (CSC) for partial financial support.

[1] Liang Pan and David B. Bogy, Nature Photonics **3**, 189 (2009).
[2] M. H. Kryder, E. C. Gage, T. W. McDaniel, W. A. Challener, R. E. Rottmayer, G. Ju, and M. F. Erden, Proceedings of the IEEE **96**, 1810 (2008).
[3] R. H. Vaictora and X. Shen, IEEE Trans. Magn. **41**, 2828 (2005).
[4] H. J. Richter, A. Y. Dobin, O. Heinonen, K. Z. Gao, R. Veerdonk, R. T. Lynch, and R. Brockie, IEEE Trans. Magn. **42**, 2255 (2006).
[5] K. Srinivasan and S.N. Piramanayagam, "Chapter 4. Perpendicular recording media," in *Developments in Data Storage: Materials Perspective*, edited by S. N. Piramanayagam and Tow C. Chong (John Wiley & Sons, 2011).
[6] B.D. Terris, J. Magn. Magn. Mater. **321**, 512 (2009).
[7] B.D. Terris and T. Thomson, J. Phys. D. Appl. Phys. **38**, R199 (2005).
[8] D. Weller and A. Moser, IEEE Trans. Magn. **35**, 4423 (1999).
[9] Roger Wood, IEEE Trans. Magn. **36**, 36 (2000).
[10] A. Perumal, Y. K. Takahashi, T. O. Seki, and K. Hono, Appl. Phys. Lett. **92**, 132508 (2008).
[11] T. Bublat and D. Goll, Nanotechnology **22**, 315301 (2011).
[12] T Seki, T Shima, K Takanashi, Y Takahashi, E Matsubara, and K Hono, IEEE Trans. Magn. **40**, 2522 (2004).
[13] T. Seki, T. Shima, K. Takanashi, Y. Takahashi, E. Matsubara, and K. Hono, Appl. Phys. Lett. **82**, 2461 (2003).
[14] JS Chena, BC Lima, YF Dinga, and GM Chow, J. Magn. Magn. Mater. **303**, 309 (2006).
[15] Tomoyuki Maeda, IEEE Trans. Magn. **41**, 3331 (2005).
[16] B. D. Terris and T. Thomson, J. Phys. D. Appl. Phys. **38**, R199 (2005).

[17] H. J. Richter, A.Y. Dobin, O. Heinonen, K.Z. Gao, R.J. M. van de Veerdonk, R.T. Lynch, J. Xue, D. Weller, P. Asselin, M.F. Erden, and R.M. Brockie, IEEE Trans. Magn. **42**, 2255 (2006).
[18] H.J. Richter, J. Phys. D. Appl. Phys. **40**, R149 (2007).
[19] S. Y. Chou, P. R. Krauss, and P. J. Renstrom, J. Vac. Sci. & Tech. B **14**, 4129 (1996).
[20] L. J. Guo, Advanced Materials **19**, 495 (2007).
[21] A. Breitling, T. Bublat, and D. Goll, Physica Status Solidi (RRL)-Rapid Research Letters **3**, 130 (2009).
[22] Q. Dong, G. Li, C. L. Ho, M. Faisal, C. W. Leung, P. W. T. Pong, and W. Y. Wong, Advanced Materials **24**, 1033 (2012).
[23] T. Bublat and D. Goll, J. Appl. Phys. **110**, 073908 (2011).
[24] Z. Li and K.M. Krishnan, J. Appl. Phys. **113**, 17B901 (2013).
[25] Z. Li, B.S. Kwon, and K.M. Krishnan, J. Appl. Phys. **115**, 17E502 (2014).
[26] www.ntt-at.com/product/Nanoimprint_custom.
[27] W. Zhang and K. M. Krishnan, J. Micromech. Microeng. **24**, 093001 (2014).
[28] W Zhang, DN Weiss, and KM Krishnan, J. Appl. Phys. **107**, 09D724 (2010).
[29] BS Kwon, Z Li, W Zhang, and KM Krishnan, J. Appl. Phys. **115**, 17B506 (2014).
[30] BS Kwon, W Zhang, Z Li, and KM Krishnan, Adv. Mater. Interfaces **2**, 1400511 (2015).
[31] W Zhang, DN Weiss, and KM Krishnan, J. Microm. & Microe. **21**, 045024 (2011).
[32] C. L. Platt, K. W. Wierman, E.B. Svedberg, R. Van de Veerdonk, J.K. Howard, A.G. Roy, and D.E. Laughlin, J. Appl. Phys. **92**, 6104 (2002).
[33] G.Q. Li, H. Takahoshi, H. Ito, H. Saito, S. Ishio, T. Shima, and K. Takanashi, J. Appl. Phys. **94**, 5672 (2003).
[34] D. Mauri, H.C. Siegmann, P.S. Bagus, and E. Kay, J. Appl. Phys. **62**, 3047 (1987).
[35] T. Klemmer, D. Hoydick, H. Okumura, B. Zhang, and W.A. Soffa, Scripta Metallurgica et Materialia **33**, 1793 (1995).
[36] T. Thomson, G. Hu, and B. D. Terris, Phys. Rev. Lett. **96**, 257204 (2006).
[37] through discussion with Dr. Bruce Terris.
[38] Rok Dittrich, Guohan Hu, Thomas Schrefl, Thomas Thomson, Dieter Suess, Bruce D. Terris, and Josef Fidler, J. App. Phys. **97**, 10J705 (2005).
[39] June W. Lau, Xiaoyong Liu, Robert C. Boling, and Justin M. Shaw, Phys. Rev. B **84**, 214427 (2011).
[40] Justin M. Shaw, Miles Olsen, June W. Lau, Michael L. Schneider, T. J. Silva, Olav Hellwig, Elizabeth Dobisz, and Bruce D. Terris, Phys. Rev. B **82**, 144437 (2010).
[41] R. Victora and X. Shen, Magn. IEEE Trans. **41**, 537 (2005).
[42] D. Eckert, J. Magn. Magn. Mater **83**, 197 (1990).
[43] J.-P. Jamet, S. Lemerle, P. Meyer, J. Ferré, B. Bartenlian, N. Bardou, C. Chappert, P. Veillet, F. Rousseaux, D. Decanini, and H. Launois, Phys. Rev. B **57**, 14320 (1998).
[44] E.F. Kneller and R. Hawig, IEEE Trans. Magn. **27**, 3588 (1991).
[45] A. T. McCallum, P. Krone, F. Springer, C. Brombacher, M. Albrecht, E. Dobisz, M. Grobis, D. Weller, and O. Hellwig, Appl. Phys. Lett. **98**, 242503 (2011).